Cement and Concrete Composites 133 (2022) 104660

Contents lists available at ScienceDirect

Cement and Concrete Composites

journal homepage: www.elsevier.com/locate/cemconcomp

Inter-laboratory study on the influence of 3D concrete printing set-ups on the bond behaviour of various reinforcements

Lukas Gebhard [a,*,1], Laura Esposito [b,1,**], Costantino Menna [b], Jaime Mata-Falcón [a]

[a] Institue of Structural Engineering, ETH Zurich, Switzerland
[b] Department of Structures for Engineering and Architecture, University of Naples Federico II, Italy

ARTICLE INFO

Keywords:
Inter-laboratory study
Digital fabrication with concrete
3D extrusion concrete printing
Interlayer reinforcement strategies
Bond behaviour

ABSTRACT

This study investigates the influence of different printing set-ups and materials on the bond strength of reinforcement manually placed between 3D printed concrete layers. An identical experimental campaign was performed at two institutes in Switzerland and Italy. Each institute used its own printing process, which consisted either of a set on-demand mix or a high yield stress material. Two types of reinforcement (reinforcing bar Ø8 mm and a high strength steel wire Ø1 mm) and three production configurations (casting and printing with the reinforcement parallel or perpendicular to the printing direction) were investigated. The results showed high bond strength with only a limited influence of the fabrication method for the reinforcing bars. An increased bond was observed for the set on-demand approach compared to the high yield strength material. The comparison with existing models showed that the reinforcing bar bond strength of printed concrete varies slightly from conventional concrete. The high strength wires exhibited poor bond. Based on the gathered experiences, insights into the standardisation of testing for 3D concrete printing are discussed.

1. Introduction

Innovative technologies are emerging in the construction industry, intending to optimise and automatise production processes. Digital Fabrication with Concrete (DFC) uses digital data to drive manufacturing equipment towards the fabrication of concrete products. The resulting workflow aims to improve productivity, efficiency and manufacturing flexibility. Such technologies could help reduce the construction industry's environmental impact [1]. 3D Concrete Printing (3DCP) [2,3] belongs to additive manufacturing technologies in the field of DFC. The most widespread 3DCP process consists of concrete layer extrusion through a nozzle attached to a robotic system (e.g. robotic arm, gantry system). 3DCP offers the advantages of eliminating the necessity of formworks to produce structural and non-structural elements with high shape flexibility, high-quality control, and reduced construction time and waste [4]. On the other hand, it faces some challenges, mainly linked to the difficulty of integrating reinforcement during the printing process, which hinder the fabrication of structural concrete members satisfying safety regulations of building codes.

Cementitious materials have a quasi-brittle mechanical response and low tensile strength. Therefore, these materials are traditionally combined with reinforcement resisting the tensile forces to produce load-bearing structures with a ductile response. However, this reinforcement inclusion is not straightforward in 3DCP due to the layered manufacturing process. A wide range of reinforcement strategies for DFC has been developed and explored over the recent years [5–8]. One promising strategy consists of reinforcement addition between extruded concrete layers (interlayer reinforcement), which can be complemented after the concrete manufacturing with a different reinforcement strategy (post-tensioning or passive reinforcement in channels) that provides resistance perpendicularly to the printing direction [9].

The reinforcement added between extruded concrete layers typically consists of conventional reinforcing bars (e.g. [10]) or flexible filaments, such as carbon filaments [11] or steel wires [12]. Determining the bond-slip behaviour between the interlayer reinforcement and the surrounding concrete is essential since it influences the mechanical performance and the reinforcement effectiveness. Pull-out tests are the most frequent method to assess the bond strength of bars in conventionally cast concrete. Those tests usually follow the RILEM recommendation [13], consisting of a single bar pulled from an uncracked cubic concrete specimen (for bars of at least 10 mm, the embedment and

* Corresponding author. Stefano-Franscini-Platz 5, 8093 Zurich, Switzerland.
** Corresponding author.
E-mail addresses: gebhard@ibk.baug.ethz.ch (L. Gebhard), laura.esposito2@unina.it (L. Esposito).
[1] both authors contributed equally to the presented manuscript.

https://doi.org/10.1016/j.cemconcomp.2022.104660
Received 23 March 2022; Received in revised form 31 May 2022; Accepted 4 July 2022
Available online 7 July 2022

Nomenclature

Abbreviations

3DCP	3D Concrete Printing
CoV	Coefficient of Variation
DFC	Digital Fabrication with Concrete
ETHZ	Institute of Structural Engineering, ETH Zurich, Switzerland
UniNa	Department of Structures for Engineering and Architecture, University of Naples Frederico II, Italy

Latin letters

A_i	Cross-sectional area of reinforcement *i*
F	Applied force
F_{max}	Maximum applied force
f_c	Concrete compressive strength
f_{cm}	Mean concrete compressive strength
f_{ct}	Concrete tensile strength
$f_{ct,fl}$	Concrete tensile strength determined with flexural tests
$f_{i,y}$	Yield stress of reinforcement *i*
$f_{i,u}$	Ultimate stress of reinforcement *i*
l_b	Bonded length

Greek letters

$\varepsilon_{i,y}$	Yielding strain of reinforcement *i*
$\varepsilon_{i,u}$	Ultimate strain of reinforcement *i*
τ_b	Bond stress
$\tau_{b,max}$	Maximum bond stress
τ_{bd}	Design value of the bond strength
$\tau_{max,good}$	Maximum bond stress for good bond conditions according to the *fib* Model Code 2010

Symbols

$\varnothing_s$	Diameter of the steel reinforcing bar
$\varnothing_w$	Diameter of the wire corresponding to the cross-sectional area of the wire

Subscript i

s	steel reinforcing bar
w	wire

side lengths are five and twenty times the diameter of the bar, respectively). Such tests provide a result of the bond strength under standard conditions that allows comparing concrete with different strength [14], reinforcement with varying rib geometries [15,16], different compaction conditions [17] and size effects [18]. The actual bond behaviour in the structure also depends on factors like cracking or confinement, which can be investigated with bending tensile tests [19] and pull-out tests in other configurations [20], particularly when using distributed fibre optical instrumentation [19,21].

The evaluation and standardisation of the bond behaviour pose many challenges in 3DCP since it is necessary to consider the particularities induced by this novel fabrication method. Indeed, there are many differences with respect to conventional concrete that may affect the resulting bond performances: (i) composition of the printable cementitious materials usually employed (which are characterised by the small aggregate and admixtures to ensure the printability requirement), (ii) anisotropy (due to the concrete layer interfaces which could present a source of weakness depending on the time gap between printed layers), (iii) specific printing parameters adopted (e.g. nozzle speed, material flow), (iv) reinforcement type, which could differ from the traditional one to meet the specific requirements of the 3D printing process.

For interlayer reinforcement with conventional reinforcing bars manually placed between adjacent layers, Baz et al. [22,23] performed various pull-out tests on reinforcing bars with a diameter of 8 mm with different material and printing parameters. They investigated the effect of varying workability (i.e. change in superplasticiser content and water to binder ratio) and the fabrication method (i.e. casting and 3D printing with the reinforcement located parallel or perpendicularly to the printing direction). For the pull-out tests, small samples were printed, and later, another mortar was cast around the specimens to produce the testing cubes. The bars were pulled out with an embedment length of 8 cm [22] or 4 cm [23]. In the first study [22], no influence on the bond behaviour by the workability or production method was found. However, in the second [23], a slight decrease in the bond strength from 18.7 MPa for cast specimens to 16.2 MPa (i.e. 13% reduction) for parallel printed and to 14.5 MPa (i.e. 22 % reduction) for perpendicular printed specimens could be observed.

The bond behaviour between steel bars with a diameter of 10 mm and 3D printed concrete was also studied by Ding et al. [24]. The research focuses on the effect of the fabrication method (i.e. casting and 3D printing with the reinforcement located parallel or perpendicularly to the printing direction), steel bar anchorage length (four, six and eight times the bar diameter), and incorporation of recycled sand and fibres. The specimens were fully printed in this study, and the reinforcement was manually placed. Before testing, the loading surface of the specimens was levelled with high-strength gypsum to ensure an even support. For specimens without fibres, recycled aggregates, and a bonded length of 40 mm, they recorded bond strengths of 25.7 MPa, 22.9 MPa and 19.3 MPa for the cast, parallel printed and perpendicular specimens, respectively. Therefore, they showed that the bond strength of the 3D printed specimens was lower than the mould-cast ones, especially for the specimen with the reinforcing bar placed perpendicular to the printing path. However, the authors stated that the differences between the two reinforcement orientations are not significant. While the specimens with the shortest embedment length had a pull-out failure, the longest embedment reached a splitting failure. Therefore, if a sufficient anchorage length is ensured, its increase does not significantly improve the pull-out load for the 3D printed concrete specimens. Furthermore, the authors detected a lower bond strength with recycled sand, but its value increased when the fibres were incorporated.

A further study on the pull-out behaviour of such a reinforcement approach was performed by Sun et al. [25]. They investigated the pull-out behaviour of BFRP bars placed between the printed concrete layers in different directions. The cubes were fully printed in their study, and a wooden frame controlled the reinforcing bar position. After production, the specimens were cut into cubes with a side length of 15 cm to ensure plane surfaces. They also observed the degradation of the bond due to the printing fabrication method.

A study by Freund and Lowke [26] explored interlayer reinforcement for sprayed 3D concrete printing. Their study investigated the influence of the accelerator content on the void spaces and the bond strength through pull-out tests on specimens with a reinforcing bar of 12 mm in diameter and a bonded length of 60 mm. The specimens were cut out of a larger element in the fresh state. Afterwards, concrete was cast around the elements in a cubic mould with a side length of 200 mm. The bond stress for 0%, 2% and 4% of accelerator dosage was 26.2 MPa, 24.7 MPa and 22.8 MPa, respectively. Their results showed that an increase in the accelerator, and therefore, in yield strength, increases void spaces around the reinforcement and reduces the bond strength. However, the bond was improved for all accelerator dosages compared to cast specimens, probably due to the high compaction achieved during the spraying process.

Bos et al. [27] performed an experimental campaign to investigate the bond behaviour of filament reinforcement. They conducted pull-out and bending tests on printed samples with two different mortars and two types of high strength wires consisting of multiple strands, which were automatically placed with the concrete filament deposition in the printing direction. They cut specimens out of the printing path before the initial set time. They observed low bond strength in pull-out tests on printed specimens (in the range of 0.4–1.6 MPa) accompanied by a large scatter of the results caused by the bonding area degradation due to (i) chemical reactions between the steel wire and the printing mortar and (ii) cavities below the wire due to the printing process. Furthermore, the average bond strength decreased with increasing bonded length [27].

In the mentioned studies, the bond behaviour of reinforcing bars in 3D printed specimens was investigated through pull-out tests. However, different approaches were followed to get representative 3D printed specimens. The pull-out samples were partially printed in [22,23,26] and successively confined with an additional mortar casting to ensure flat surfaces and similar dimensions as standard pull-out tests. Instead, the specimens were fully printed in [24] and successively levelled with gypsum to ensure plane loading surfaces. Another solution was presented in [25], in which the specimens were entirely printed and successively cut into cubes. Another critical aspect is the time gap to place reinforcement and print above it. In [22,23], the reinforcement was placed within the time gap between two consecutive layers, while there are no details on this aspect in [24,25].

The chosen printing strategy (i.e. the use of a high yield stress mortar or a set on-demand system with accelerated hydration) might influence the bond behaviour of the reinforcement due to the very different consistency of the mortar coming out of the nozzle. However, this influence has not been compared under homogeneous conditions. Since there are not yet standardised procedures in the 3DCP production process, the entire evaluation of the bond behaviour, including the specimen preparation and the reinforcement incorporation, is strongly influenced by the printing parameters (printing set-up, material, print path, print speed, print geometry etc.). In this framework, inter-laboratory studies are needed to investigate such influence, comparing the experimental outcomes and helping the testing procedures standardisation.

2. Research relevance

Existing research on the bond behaviour in 3DCP applications is limited. Moreover, the influence of the printing system is unknown since previous studies used different reinforcements and testing procedures for the same printing set-up. This study discusses the results of an interlaboratory study on the bond behaviour of two reinforcements (steel reinforcing bars and wires) embedded between extruded printed layers using two different printing systems: The bond behaviour when using a stiff and thixotropic mortar (at the Department of Structures for Engineering and Architecture at the University of Naples Federico II in Italy, UniNa) is compared to the one using a set on-demand system [28] (at the Institute of Structural Engineering at ETH Zurich in Switzerland, ETHZ). The two reinforcement approaches were chosen since they both provide continuous reinforcement and have both been used for structural applications using 3DCP [9]. While the cable offers flexibility during printing, conventional deformed steel bars provide better ductility and a higher load-bearing capacity. Therefore, the bond is an important factor in further discussing the advantages and drawbacks of these two strategies. Three fabrication methods were studied at each laboratory: casting, parallel printing and perpendicular printing. Identical reinforcement, printing parameters and testing procedures were employed to ensure consistency among the two institutions. The testing consisted of pull-out tests following the RILEM recommendations [19]. Each printed specimen was produced adopting the printing-inside-formwork approach to ensure planar surfaces (i.e. loading areas during the test execution) and control the reinforcement location. The experience gained in this interlaboratory study provides insights into the opportunities and challenges of standardising methods in the bond strength measurement for reinforcement placed between the layers, addressing various critical points for a successful implementation of interlaboratory studies in the field of 3DCP. For the implantation of reinforcement placed between the layers, further aspects such as durability need to be considered. However, this active field of research is out of scope for the presented paper.

3. Material and methods

3.1. Overview

The experimental campaign consisted of 60 pull-out tests (30 tests in each institute) performed by varying (i) the reinforcement type (bar (R), wire (W)), (ii) the specimen fabrication method (cast (C) and 3D printing (3D).) and (iii) the relative orientation between the printed layer and the reinforcement (parallel || and perpendicular ⊥). Each pull-out specimen was prepared according to the RILEM recommendations [13]. However, the specimens' size and the bonded length value were slightly adapted (i.e. reduced bonded length for the reinforcing bars and increased bonded length for the wire reinforcement). The specimens had a cubic shape with a side length of 200 mm. Two different printable cementitious materials were used (see Section 3.2). Either a conventional reinforcing bar with a diameter of 8 mm or a high strength steel wire with a nominal diameter of 1 mm were placed in the centre of the cube with a bonded length l_b of four and fifty times the diameter, respectively (see details of the reinforcement in Section 3.3). The bonded lengths were chosen to ensure a sufficiently large embedment while avoiding yielding of the reinforcement. A pilot series was performed to ensure that the selected parameters were adequate. Furthermore, the reinforcement material was shipped from one institute to the other to ensure consistency.

Reference cast specimens were prepared by filling a mould with the material coming off the nozzle. The printing-in-formwork approach was employed to prepare the 3DCP pull-out specimens; it allowed smooth surfaces for testing and controlled sizes and geometries. The production process consisted of (i) printing the first 100 mm, (ii) pausing the print for around 5.5 min to manually place the reinforcement and (iii) printing the second half of the specimens. Five specimens were produced together to provide a representative set for each fabrication method. Directly after printing, the specimens were separated to avoid the need for cutting at the hardened state. A total of fifteen cubic specimens for each reinforcement strategy and institute were prepared in a single printing session.

For the mechanical characterisation of the printing material, six cylinders (300 mm × 150 mm) were filled during the printing session, with the extruded mortar and without applying any compaction. The cylinders were tested under compression and indirect tension at 28 days (see Section 3.2.2). The pull-out tests were performed after 28 days, and for each specimen, the force and slip were recorded (see Section 3.5 for further details).

For each fabrication method, small prisms (40 × 40 × 160 mm) were cut out from one of the five tested specimens to perform additional material characterisations, including the layering effect (see Section 3.2.3). These tests were repeated in untested specimens for both 3D printed configurations with reinforcing bars to compare the results between tested and untested specimens. Furthermore, some specimens with reinforcing bars were cut along the bar and through the cross-section to visually inspect the interface between steel and concrete (see Section 3.6). An overview of the test matrix is given in Table 1.

3.2. Printable cementitious mortars

A cement-based material should satisfy pumpability, extrudability and buildability requirements to meet the critical prerequisites of a freeform construction process [29] having specific mechanical and rheological properties [30,31]. In particular, there are two kinds of cementitious materials usually adopted in 3DCP applications: mortars

Table 1
Overview of the testing campaign (N: UniNa, Z: ETHZ, R: Reinforcing bar, W: Wire reinforcement, C: Cast, 3D: 3D concrete printed,||: parallel configuration,⊥: perpendicular configuration).

Institute	Reinforcement	Fabrication	Layer orientation	Nomenclature	# Pull out specimens	# Prisms cut out from	
						tested specimens	untested specimens
N	R	C	–	N-R-C	5	3	–
Z				Z-R-C	5	3	–
N		3D	Parallel	N-R–3D‖	5	3	3
Z				Z-R–3D‖	5	3	3
N		3D	Perpendicular	N-R–3D⊥	5	3	3
Z				Z-R–3D⊥	5	–	3
N	W	C	–	N–W–C	5	3	–
Z				Z-W-C	5	3	–
N		3D	Parallel	N–W–3D‖	5	3	–
Z				Z-W–3D‖	5	–	–
N		3D	Perpendicular	N–W–3D⊥	5	3	–
Z				Z-W–3D⊥	5	3	–

with low or high initial yield stress. The first kind of material is employed in a set on-demand [28] process, and it is characterised by a low initial yield strength facilitating extrudability and pumpability but limiting buildability. Therefore, the concrete is usually mixed with an accelerator agent right before the extrusion. As a result, the setting and hardening of a retarded batch are accelerated and controlled by adjusting the accelerator amount. On the contrary, the other approach is based on thixotropic material with a yield strength high enough to ensure buildability but not too high to simultaneously guarantee the pumpability and extrudability requirements.

The cementitious mortars employed in this experimental campaign were developed by Italcementi-Heidelberg Cement for UniNa and internally developed at ETHZ, satisfying all printability requirements. The UniNa cement-based material is a high yield stress mortar with a maximum aggregate size of 2 mm, whereas the ETHZ mortar with a maximum aggregate size of 1.2 mm is controlled by set on-demand.

3.2.1. Fresh state properties

The mortar of UniNa exhibited static yield stress of over 50 kPa measured with a Stress Growth Test and over 4 kPa measured with a Penetration Test. The setting times were estimated according to the EN 196–3:2017 [32] range from 120 ± 10 min to 180 ± 10 min. Instead, the non-accelerated ETHZ mortar typically had a spread on the flow table (ASTM C 1437 [33]) of 130–150 mm without strokes. According to the model of Pierre et al. [34], this is the same as having a dynamic yield stress of approximately 0.2 kPa and is measured after extrusion. By vane rotational rheometry (ramp 50 to 10 1/s), typical values for dynamic yield stress lay in the range of 0.3–0.6 kPa (self-support 22 mm–45 mm). After 2 min at rest, the static yield stress was in the range of 0.7–1.5 kPa (also by vane rheometry and equivalent to 52 mm–110 mm). The typical thixotropic build-up/structuration rate of the accelerated mortar lay in the range of 100–400 kPa/h by penetration tests (depending on accelerator dosage). However, the mortar formulation in this study exhibited a short timeframe after acceleration in which no substantial thixotropic build-up is observed from the accelerator, typically in the range of 2–3 min, and the accelerator did not substantially change the dynamic yield stress at the time of extrusion.

3.2.2. Hardened state properties of the bulk materials

The printable material's hardened properties were measured through three uniaxial compressive tests (EN 12390–3:2009 [35]) and three splitting tests (ASTM C 496–96 [36], Brazilian tests) after 28 days. Therefore, six cylinders with a diameter of 150 mm and a height of 300 mm were cast with the extruded material for each printing session (see Table 2) without compaction. A total of 12 cylinders were tested at each institute. Table 2 illustrates the average compressive f_c and tensile f_{ct} strength of the printable mortars adopted in this study. The ETHZ mortar showed higher compressive strength (about 26%) than the UniNa one.

Table 2
Overview of the mechanical characterisation at 28 days of the two mortars from cast samples.

Laboratory	Printing session	f_c [MPa] (CoV)	f_{ct} [MPa] (CoV)
UniNa	(A) with wire	46.4 (17%)	3.8 (12%)
	(B) with bar	40.1 (11%)	2.9 (18%)
ETHZ	(A) with wire	52.8 (1%)	3.2 (15%)
	(B) with bar	56.3 (2%)	2.7 (26%)

Furthermore, experimental outcomes reveal a percentage variation of about 6% and 14% (at UniNa and ETHZ, respectively) in the compressive strength of the same mortar measured from two different printing sessions (i.e. (A) wire vs (B) bar in Table 2).

3.2.3. Hardened state properties of cut printed samples

In addition to the mechanical characterisation of the bulk printable mortar, prism samples of 40 × 40 × 160 mm (Fig. 1a) were cut from tested and untested pull-out specimens. These tests allowed studying the influence of layered production on the mechanical properties of the mortar. In some cases, no prisms were obtained since the interface cracked during cutting. The available samples, including cast and printed specimens, are listed in Table 1. Three-point bending and compression tests [37] were carried out on the prisms to quantify the flexural and compressive strength (Fig. 1b). The prisms were tested in bending with the interface where the reinforcement was placed at midspan (see Fig. 1b). This interface is characterised by the longest interval time (due to the reinforcement placing procedure). Therefore, the resultant flexural strength is representative of the middle section of the pull-out specimens, which is assumed to be the weakest.

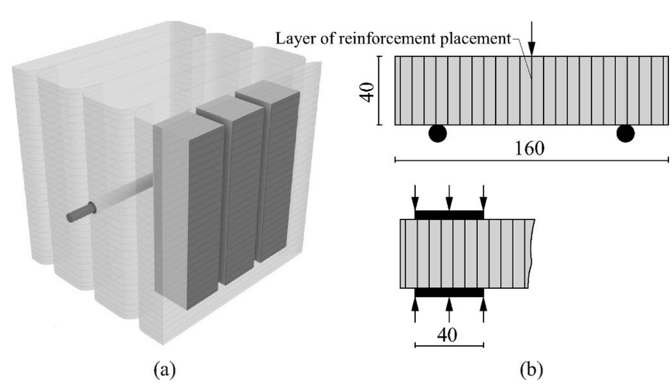

Fig. 1. Prisms for material tests cut from pull-out specimens: (a) illustration of the three prisms cut out from one specimen (exemplary for the parallel printing configuration); (b) three-point bending and compression testing set-ups according to EN 196–1:2016.

In addition to extracting samples from tested pull-out specimens, a set of 3D printed pull-out specimens with reinforcing bars was prepared in a separate printing session and reserved to cut samples without testing influence. These samples were helpful to evaluate the pull-out testing influence on the middle interface and study the steel-concrete interface in an undamaged state (see Section 3.6). The comparison between tested and untested samples investigated whether the reduced bending strength in the middle interface was due to its longest time gap or due to possible cracking developed during the pull-out test. Note that no untested samples were cut from wire-reinforced specimens since it was assumed that the low pull-out force of the wire does not affect the interlayer.

A summary of the results is shown in Table 3. In some cases, the pull-out tested specimen cracked before or during the cutting and no specimens were obtained (i.e. Z-R-3D⊥ and Z-W-3D||). From Table 3, it is possible to observe that ETHZ mortar provided higher compressive and flexural strength, confirming the experimental results on cast cylinders previously discussed (see Table 2).

At UniNa and ETHZ, the difference in flexural strength between tested and untested specimens is contained in the experimental scatter, especially considering that these specimens were produced in different printing sessions. On the contrary, the difference between printed and cast specimens of the same printing session results in a considerable reduction of the bending tensile strength of 32% and 37% at UniNa and ETHZ, respectively. The average flexural tensile strength of all small prism specimens from UniNa and ETHZ was 4.5 MPa and 5.9 MPa, respectively. Compared to the cast cylinders, these values present an increase of 33% and 102%. The differences between the measured values might be mainly caused by the different techniques (i.e. splitting test vs 3-point bending test).

For the compressive strength, no significant influence of neither printing nor testing could be observed as the differences in strength are contained in the experimental scatter. This observation of the hardened printed material follows the findings made by other authors [38].

3.3. Steel reinforcement

The steel bars had a diameter of 8 mm and a relative rib area (i.e. rib index) of 0.078. The reinforcing bars had a thread at the end, allowing anchorage during testing. The mechanical properties of the reinforcing bars were obtained by direct tension tests based on the EN ISO 6892–1:2016 on three samples. The resulting stress-strain curves and characteristic dynamic values are shown in Fig. 2 a.

For the reinforcing bar, the yield stress ($f_{s,y}$) was 529 MPa with a yielding strain ($\varepsilon_{s,y}$) of 2.8‰. On average, the ultimate stress ($f_{s,u}$) of 634 MPa was reached at a strain ($\varepsilon_{s,u}$) of 79.8‰. Details of the steel wire are shown in Fig. 2 b. The wire was constructed with 19 small strands with a

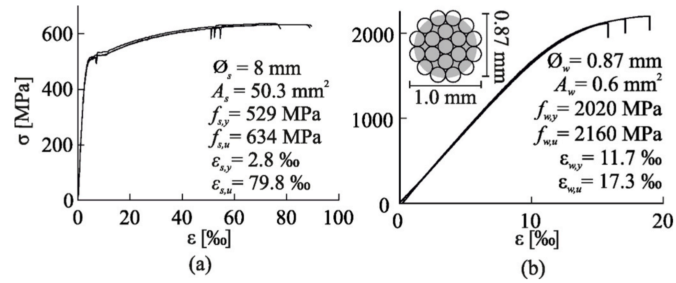

Fig. 2. Stress-strain relationship of the reinforcing steel: (a) bars and (b) wires.

cross-sectional area (A_w) of 0.6 mm^2. It is the same wire used in another study by Gebhard et al. [9]. The composition of multiple small wires makes determining the contact area with the surrounding concrete difficult. The outer envelope of the wire was ca. 1.0 mm in diameter, but the wire was modelled as a cylindrical steel element with the corresponding cross-section resulting in an equivalent diameter ($\varnothing_w$) of 0.87 mm (grey area in Fig. 2b). The yield strength ($f_{w,y}$) was 2020 MPa with a strain ($\varepsilon_{w,y}$) of 11.7‰. On average, the ultimate strength occurred at stress ($f_{w,u}$) of 2160 MPa and a strain ($\varepsilon_{w,u}$) of 17.3‰.

3.4. Production

Following the RILEM guidelines [13], part of the reinforcement was isolated to ensure bond only over a specific length. For the reinforcing bars, pipes with an outer diameter of 12 mm and an inner diameter of 10 mm were used. In contrast, pipes with an outer diameter of 4 and an inner diameter of 2 mm isolated the wire. The bonded length of the reinforcing bars was set at 32 mm (i.e. four times the diameter). While the RILEM recommendation proposes an embedment length of five times the bar diameter, a pilot test series showed that this embedment might result in the bars yielding before being pulled out. The embedment length of the wire reinforcement was 50 mm (i.e. fifty times the nominal diameter). This high value was chosen since the wire bond strength was expected to be low [27] and its yield strength high. Both reinforcements were isolated on both ends to avoid the regions in which the printing direction changes close to the formwork. Two types of printing systems were used to produce the pull-out specimens.

The system at UniNa consisted of an “m-tec duo mix 2000” pump with integrated mixing. From this pump, the material was delivered to the nozzle and extruded. As a printing platform, an ABB robotic arm was used (see Fig. 3a). At ETHZ, a continuous mixer premixed the material before depositing it inside a progressive cavity pump. Through a hose, the material was delivered to the nozzle attached to an ABB robotic arm. The accelerator was added to the mortar at the nozzle and mixed in a

Table 3
Results of the material characterisation of prism samples cut from the specimens ($f_{ct,fl}$: tensile strength of the concrete determined with flexural tests, f_c: compressive strength of the concrete).

Codification	$f_{ct,fl}$ [MPa]	$f_{ct,fl}$ [MPa]	f_c [MPa]	f_c [MPa]	Codification	$f_{ct,fl}$ [MPa]	f_c [MPa]
	(CoV)	(CoV)	(CoV)	(CoV)		(CoV)	(CoV)
Configuration	Tested	Untested	Tested	Untested		Tested	Tested
N-R-C	4.7 (6%)	– –	51.6 (5%)	– –	**N–W–C**	6.5 (3%)	49.6 (7%)
N-R-3D||	3.5 (18%)	4.0 (7%)	54.5 (4%)	47.9 (10%)	**N–W-3D||**	4.6 (3%)	50.5 (8%)
N-R-3D⊥	4.1 (5%)	4.5 (6%)	53.3 (7%)	49.2 (8%)	**N–W-3D⊥**	4.2 (11%)	55.0 (6%)
Z-R-C	7.9 (16%)	– –	63.1 (5%)	– –	**Z-W-C**	4.9 (4%)	56.6 (5%)
Z-R-3D||	5.0 (13%)	6.7 (12%)	62.2 (8%)	61.8 (6%)	**Z-W-3D||**	cracked (3%)	cracked (8%)
Z-R-3D⊥	cracked (5%)	6.1 (24%)	cracked (7%)	61.6 (3%)	**Z-W-3D⊥**	4.8 (26%)	58.6 (3%)

(a) (b)

Fig. 3. 3D concrete printing set-ups including the pumping system: (a) UniNa and (b) ETHZ.

chamber before extrusion (see Fig. 3b). A scheme of the 3DCP production can be found in [39]. At both institutes, the length of the nozzle was larger than 200 mm to allow printing inside the formwork.

Two fabrication methods (i.e. casting and printing) were used to fabricate the specimens. The reinforcement and the isolation were arranged inside formwork for the cast specimens before pouring the material coming from the nozzle. For the stiffer UniNa thixotropic mortar, only slight manual compaction with rods was applied during the casting, while at ETHZ, no compaction method was required. For the compaction, a wooden rod was used to reduce the thixotropic build-up of the mortar while filling the moulds. For the cast wire reinforced specimens, especially with the stiff material (i.e. UniNa mortar), it was challenging to ensure the straightness of the wire during casting. For the printed specimens, the sequence of production can be seen in Fig. 4. First, the formwork for five specimens was placed and fixed in the proximity of the robot (Fig. 4a). Afterwards, the first 100 mm were printed with a layer height of 7 mm and a filament width of 30 mm. The first layer height was increased to 9 mm to ensure that 100 mm would be reached precisely. A different value of the linear printing speed was adopted at ETHZ and at UniNa (i.e. on average 80 mm/s and 240 mm/s, respectively, with a corresponding time gap of around 115 s and 38 s between consecutive layers) due to the different pumping systems and flow rates. The printing speed needed to be slightly adjusted to ensure the correct filament width during printing because of slight variations in material consistency.

After the first 100 mm were produced, the printing was stopped, and the reinforcement was manually added (Fig. 4b). The formworks had large holes on both sides, with the lower edge of the holes ensuring that the reinforcement would be placed at the centre of the cubes. These holes ensured that the reinforcement could be added with minimal interference with the concrete, in the correct location and perfectly even. The time to place the reinforcement was set as 5.5 min for both institutes. This time interval was chosen to allow enough time to place the reinforcement and simulate the fabrication of a larger structure. The time increased to 9 min during the wire reinforcement placement to produce the parallel configuration at ETHZ.

After the reinforcement was placed, the next 100 mm were printed to reach the final height of 200 mm. Small vertical gaps between the formwork wall were provided to cut the specimens into cubes (Fig. 4c).

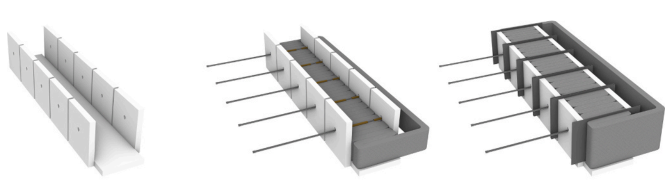

(a) (b) (c)

Fig. 4. Specimen preparation with reinforcing bars: (a) placement of the formwork; (b) printing of the first 100 mm and placement of the reinforcing bars; (c) printing of the remaining 100 mm and cutting of the specimens.

Due to the fast-hardening material, it was necessary to perform multiple cuts at ETHZ during the printing for the accelerated mix. After production, the specimens were covered with a plastic foil and left for curing at the room temperature and humidity of the respective laboratory to ensure the same curing conditions as when 3D printing large scale structural components, and tested after 28 days.

Two printing paths (Fig. 5) were used to produce the 3D printed specimens with the reinforcement aligned with the printing direction or perpendicularly. For the parallel configuration, the extruder oscillated between the two sides of the formwork over the entire length. Afterwards, it moved back to the starting position outside of the formwork. The extruder oscillated over the entire length of all five samples for the perpendicular configuration and moved back outside the formwork.

Fig. 6a to d shows the printing process for all configurations after the reinforcement placement. Minor variations in the material consistency and, hence, the flow rate, together with the formwork restrains, produced material accumulation in some cases. This accumulation led to some disturbance of the concrete surface during the reinforcement placing and the reinforcement being submerged by up to the full diameter instead of the half a diameter initially planned. Directly after printing, the formworks were clamped to ensure perpendicularity (see Fig. 6e). After demoulding, the specimens had smooth surfaces with the reinforcement perpendicular to the surface (see Fig. 6f). For the specimens with the parallel printing, the change in the direction of the robot left some voids locally between adjacent filaments. However, the outer

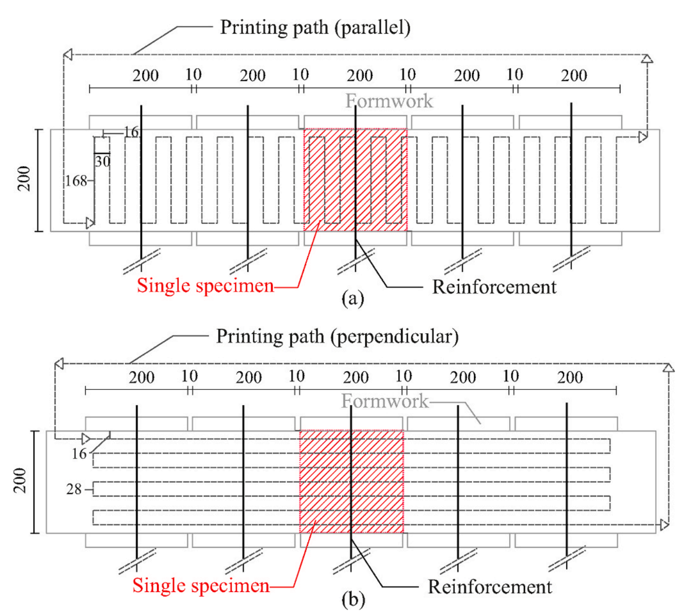

Fig. 5. Printing path of the two configurations: (a) parallel printing path; (b) perpendicular printing path.

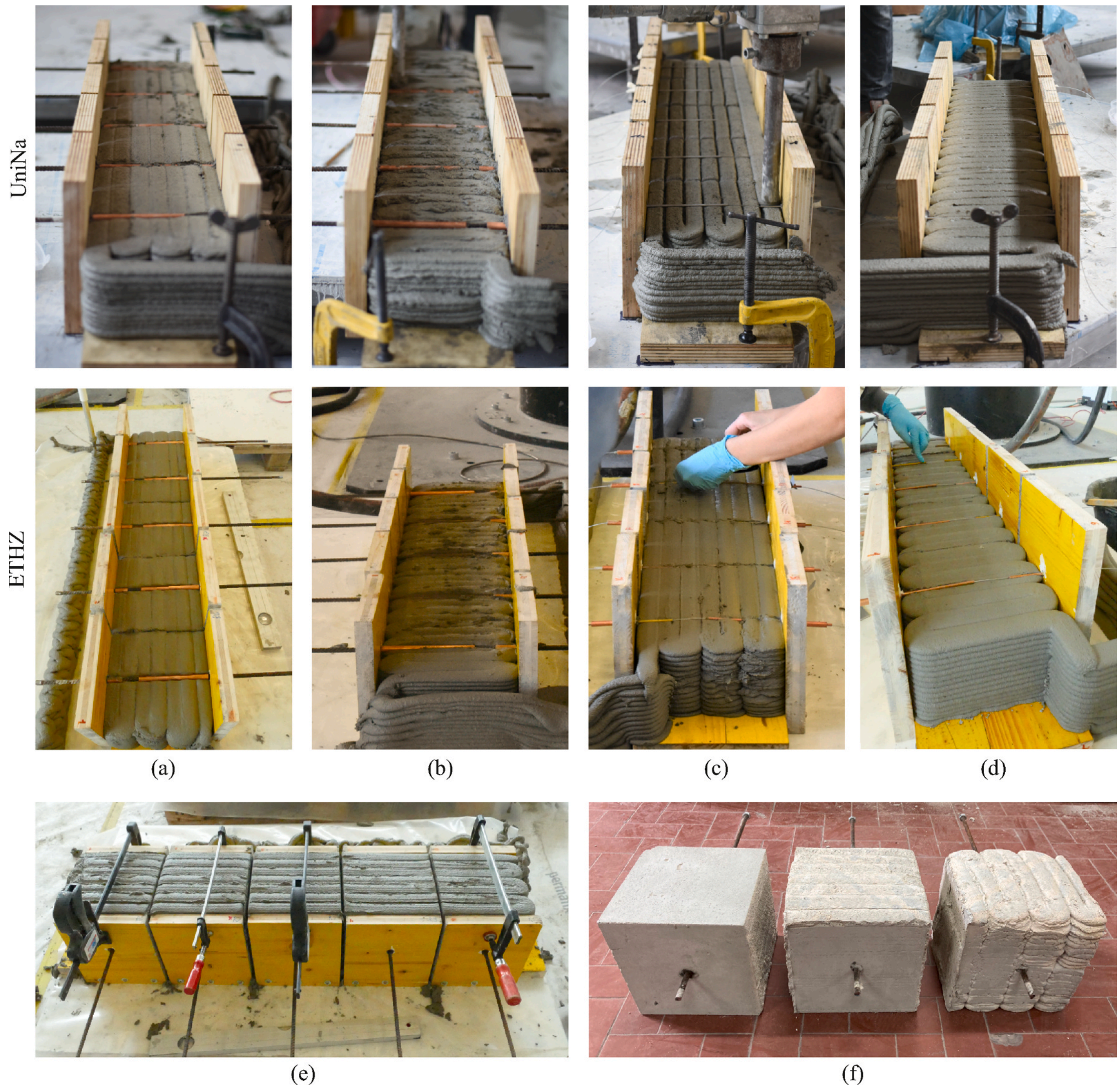

Fig. 6. Images from the production of the printed samples: (a) specimens with reinforcing bars and perpendicular configuration; (b) specimens with reinforcing bars and parallel configuration; (c) specimens with wire reinforcement and perpendicular configuration; (d) specimens with wire reinforcement and parallel configuration; (e) clamping of the formwork to ensure perpendicular; (f) demoulded specimens before testing: (ltr) cast, perpendicular and parallel.

surface was flat, and it was not necessary to further process it.

3.5. Test set-up and instrumentation

The pull-out tests were carried out on printed and cast specimens after 28 days from production in both laboratories. Figs. 7 and 8 show the scheme of the testing set-up and the corresponding pictures from both institutes for the bar and wire reinforced specimens. Steel frames held the specimen in both cases while the reinforcement was pulled. A rubber support was placed between the bearing steel plate and the specimen to ensure a uniform stress distribution. At both institutes, the applied load and the displacement of the unloaded ends (i.e. passive slip) were recorded. In Section 4, the average bond-slip curves (i.e. the average force/stress for the same slip value) will be reported for each specimen set together with the results of the individual specimen. However, the bond strength $\tau_{b,max}$ of a certain configuration will be calculated as the average of the peak force recorded for each specimen. The bond stress in the specimens with a reinforcing bar was evaluated as the ratio between the pull-out force F and the nominal contact surface determined by the bonded length l_b and the diameter of the reinforcing bar $\varnothing_s$ [13]:

$$\tau_b = \frac{F}{l_b \cdot \pi \cdot \varnothing_i} \quad (1)$$

The equivalent diameter in the specimens reinforced with wires (see Section 3.3) was used to determine the bond stresses. However, the pull-out force normalised with the bonded length (i.e. the ratio F/l_b [N/mm]) was selected as the representative variable for comparison, given the difficulty of defining the nominal contact surface of the wire reliably.

At UniNa, the fixation of the LVDT on the specimen was not possible due to the set-up. Therefore, two LVDTs were used to measure the displacement of the specimen and the displacement of the reinforcement from concrete separately (Fig. 7a). The difference between these two values gives the actual slip. For an accurate measurement of the wire-reinforced specimens, a spring-loaded LVDT was used (Fig. 8a), which applied a slight tensioning to the unloaded end of the wire. An LVDT was attached at ETHZ to the concrete specimen recording the relative displacement between the reinforcement and the surrounding concrete to measure the passive slip. A spring-loaded LVDT was also used at ETHZ for the wire reinforcement. At UniNa, an “MTS 810” universal testing machine of 500 kN was used. The MTS was equipped with an external loading cell with a capacity of 10 kN for the wire reinforcement. At

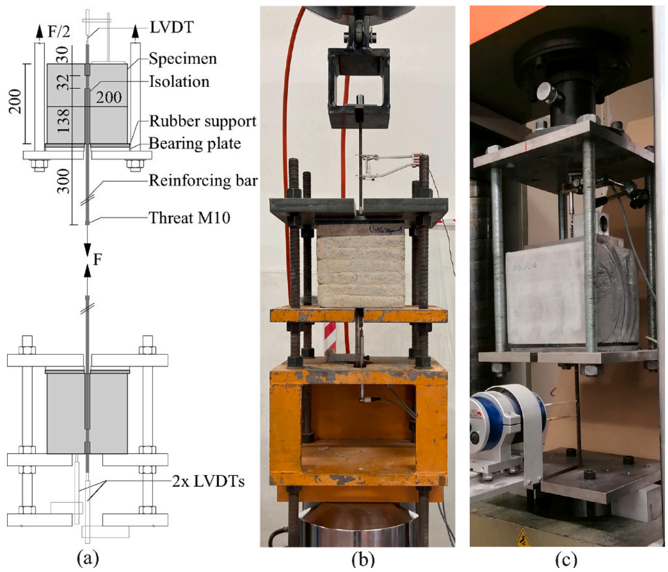

Fig. 7. Testing set-up for the pull-out tests with reinforcing bars (dimensions in [mm]): (a) testing set-up schemes (top: ETHZ, bottom: UniNa); (b) image of the test set-up at ETHZ; (c) image of the test set-up at UniNa.

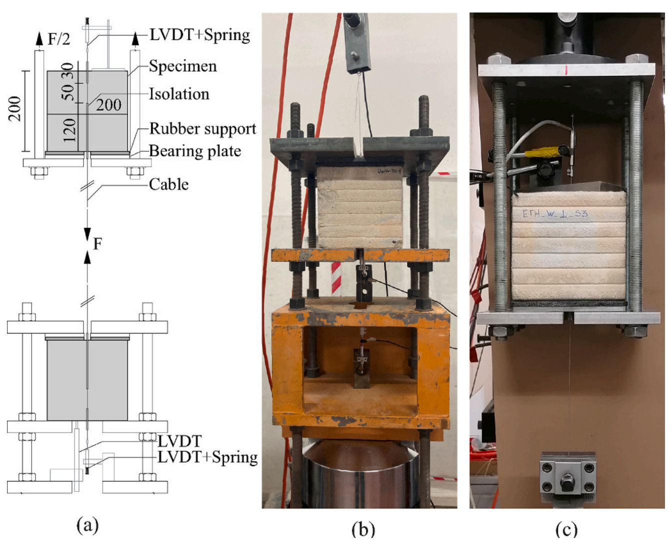

Fig. 8. Testing set-up for the pull-out tests with wire reinforcement (dimensions in [mm]): (a) testing set-up schemes (top: ETHZ, bottom: UniNa); (b) image of the test set-up at ETHZ; (c) image of the test set-up at UniNa.

ETHZ, the pull-out tests were carried out with a “Zwick Roell 1484” universal testing machine with a 200 kN capacity in a displacement-control mode. A displacement rate of 0.6 mm/min was adopted in both laboratories for both reinforcement types.

3.6. Interface inspection

The steel-concrete interface was examined by cutting tested and untested specimens. In particular, the untested specimens were cut to see the production influence on the reinforcing bar embedment (e.g. air entrapments due to printing). The bonded length was increased to 100 mm for such specimens to increase the inspectable area. Moreover, the tested specimens were used to reveal the pull-out testing influence of the reinforcing bar on the surrounding concrete (e.g. cracks in the cementitious matrix). For each printing configuration, one untested specimen was cut along the reinforcing bar (Fig. 9a) and another specimen

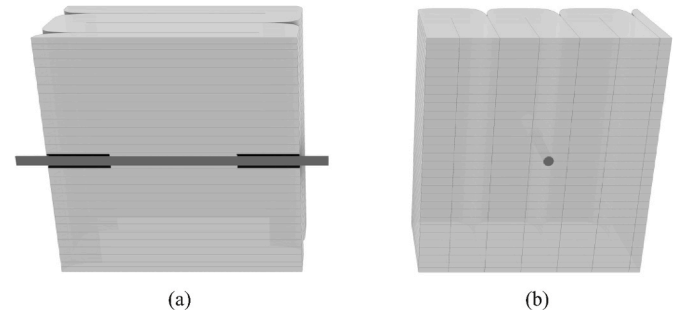

Fig. 9. Schematic view of the sections for an untested specimen with parallel printing configuration: (a) cutting along the midsection of the reinforcing bar; (b) cutting through the cross-section of the reinforcing bar.

perpendicularly to the reinforcing bar (Fig. 9b). The cut along the reinforcing bar was also performed on a perpendicular and parallel printed tested specimen. No cutting for inspection was performed on any specimens containing a wire due to the small diameter.

4. Pull-out behaviour of reinforcing bar samples

4.1. Overview

Table 4 and Fig. 10 give an overview of the average peak bond strength obtained in the pull-out tests ($\tau_{b,max}$) and the coefficient of variation (CoV) for the specimens with reinforcing bars. The average bond strength ranged from 15.4 to 19.3 MPa and from 29.7 to 30.6 MPa, for the printing system and material of UniNa and ETHZ, respectively. At UniNa, the bond strength of specimens with the reinforcement parallel to the printing direction was on average ca. 25% lower than in the cast specimens. However, such a reduction might not be significant due to the higher bond strength scatter in the parallel printed set (i.e. CoV = 31%). No differences were observed between the perpendicular printing and the cast configurations. At ETHZ, no significant differences in the bond strength between cast and printed specimens were observed. In addition to the maximum achieved bond, the actual bond-slip behaviour is an important aspect discussed in Section 4.2.

4.2. Bond slip behaviour

Fig. 11 illustrates the slip vs bond stress response for each configuration of the pull-out specimens, i.e. (a) cast, (b) printed with reinforcement parallel to the printing direction and (c) printed with reinforcement perpendicular to the printing direction. The black curves show the average result, while the light grey curves depict the outcome of each specimen. All configurations exhibited the same overall pull-out behaviour: an initial activation phase with a minimal slip until the peak bond stress was reached, followed by a phase in which the bar is pulled out from the surrounding mortar with increasing slip and decreasing resistance. The observed behaviour coincides well with the stages for pull-out behaviour of conventional reinforced concrete described in the *fib* Bulletin No. 10 [40]. There seems to be no influence of the fabrication method on the overall pull-out behaviour. The obtained slip-stress curves with smooth softening indicate that the failure was dominated by pull-out and not splitting, which agrees with the inspection of the samples cut from tested specimens (see Section 4.3). Overall the samples

Table 4
Overview of pull-out test results.

Codification	N-R-C	N-R-3D‖	N-R-3D⊥	Z-R-C	Z-R-3D‖	Z-R-3D⊥
$\tau_{b,max}$ [MPa] (CoV)	19.3 (12%)	15.4 (31%)	18.8 (13%)	29.7 (4%)	30.0 (15%)	30.6 (7%)

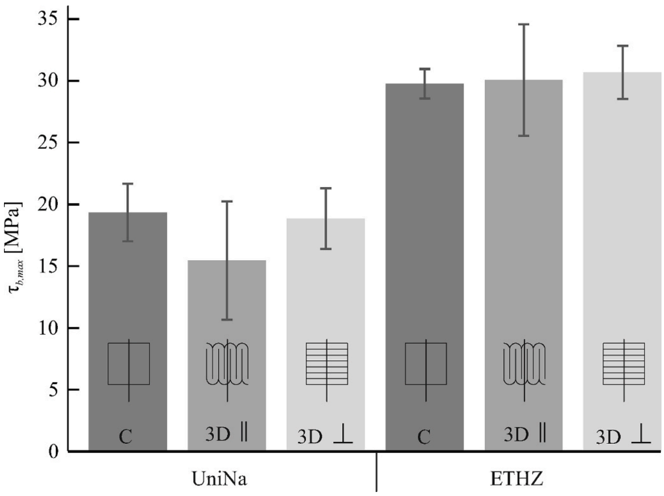

Fig. 10. Graphical representation of the pull-out tests' mean strength and coefficient of variation for all specimens with reinforcing bars.

showed a similar scatter except for some outliers occurring at both institutes for the parallel printing configuration. Since the maximum bond strength and the bond-slip relationship are directly related to how the reinforcing bars are embedded in the concrete, the quality of the steel-concrete interface is studied in Section 4.3.

4.3. Interface inspection

A visual inspection of the interface between the concrete and the reinforcing bar was performed to investigate the influence of (i) the printing configuration on the reinforcing bar embedment and (ii) the reinforcing bar activation on the surrounding concrete (i.e. potential formation of splitting cracks). The inspection of the untested specimens was achieved by cutting along the reinforcing bar (Section I in Fig. 12) and perpendicular to the reinforcing bar (Section II in Fig. 12). It is possible to observe that no significant air entrapments or voids around the reinforcing bar can be observed at UniNa. On the contrary, at ETHZ, large voids are visible in the printing close to the reinforcing bar; however, only small voids are visible in the reinforcing bar proximity. At both institutes, the embedment due to the printing process seemed adequate. Fig. 13 shows the interface of tested specimens and the damage due to bar pull-out (note that the dark area around the reinforcing bar in the parallel printing configuration of ETHZ resulted from the water during cutting and not due to a printing artefact). The inspection of the tested specimens did not yield evidence of internal or splitting cracks, showing that the splitting stress generated by the bond did not exceed the tensile strength of the mortar. Therefore, the bar was pulled out due to concrete failure at the ribs' height and a change from rib bearing to friction. As a result, the slip arose from the local crushing or shearing of the mortar near the ribs. While for conventional concrete, failure mechanisms at the interface are properly understood, the role of weak interfaces between layers and aggregate size must be investigated at a microscopic scale (e.g., CT scan) to clarify the influence of local failures.

4.4. Discussion

The experimental results have shown similar performance in the bond behaviour of printed specimens compared to the cast ones in both institutes, except for some samples which showed reduced strength (probably due to artefacts, as discussed further below). The measured bond strength at UniNa coincides well with the study of Baz et al. [23] with a different pull-out set-up, which recorded 18.7 MPa, 16.2 MPa and 14.5 MPa of bond strength for the cast, parallel printed and perpendicular printed specimen, respectively. This similarity could be expected since the work by Baz et al. also relies on the printing of a high yield stress mortar with a maximum aggregate size of 2 mm. The bond strength obtained from printing with the material and printing set-up from ETHZ resulted in significantly higher bond strength than at

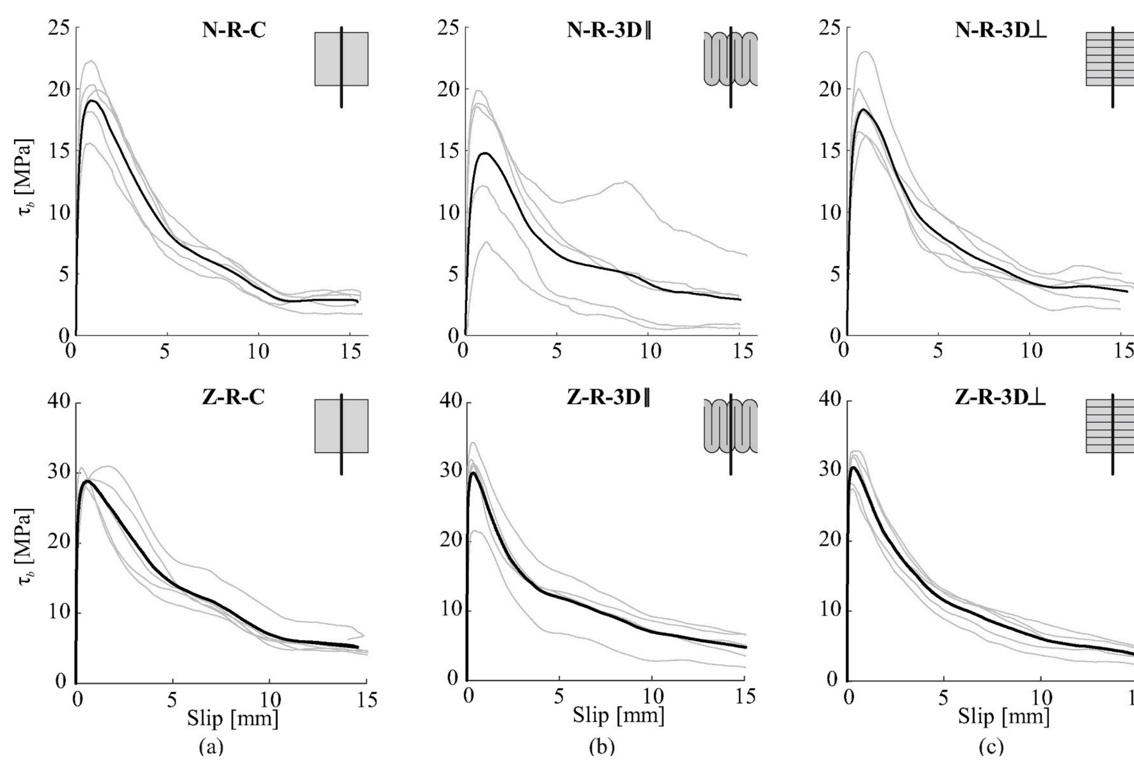

Fig. 11. Bond slip behaviour of the pull-out tests with reinforcing bars (top: UniNa printing set-up; bottom: ETHZ printing set-up): (a) cast specimens; (b) 3D printed specimens with the parallel configuration; (c) 3D printed specimens with the perpendicular configuration.

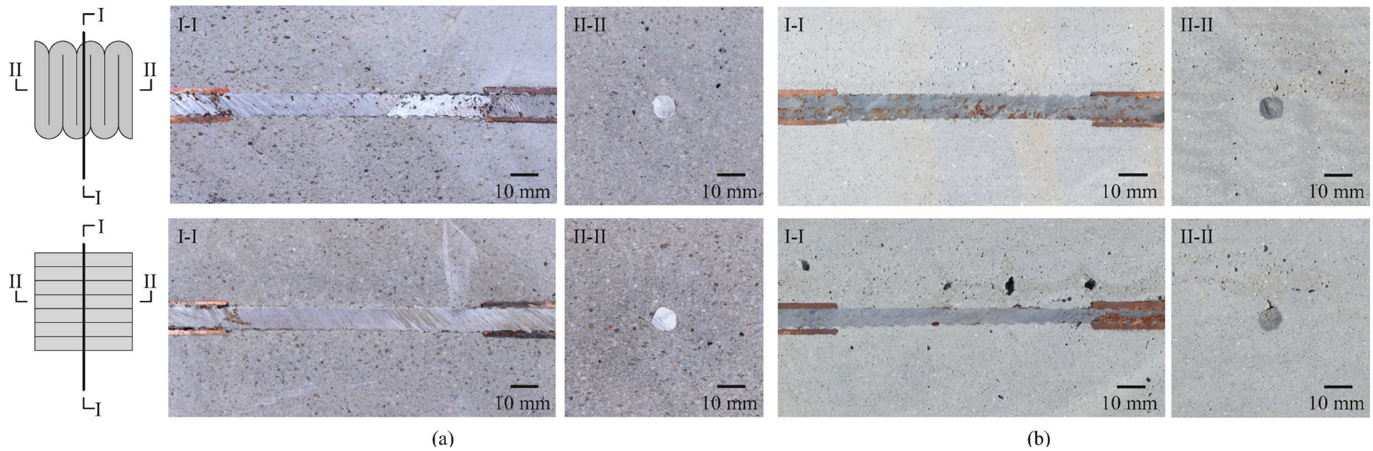

Fig. 12. Sections through the reinforcing bar in untested specimens (top: parallel configuration; bottom: perpendicular configuration): (a) UniNa; (b) ETHZ.

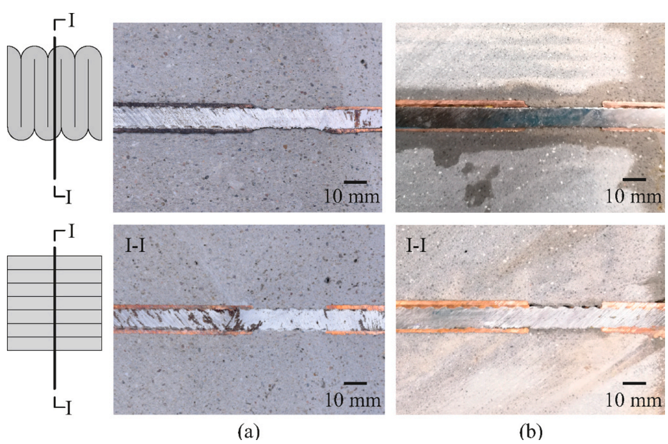

Fig. 13. Sections through the reinforcing bar in tested specimens for both printing configurations: (a) UniNa; (b) ETHZ.

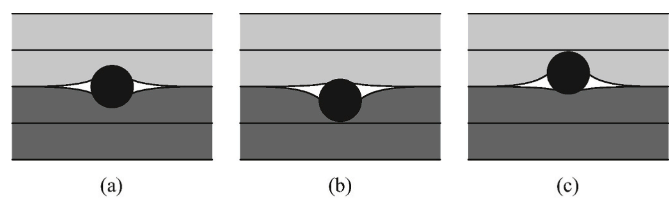

Fig. 14. Schematic representation of possible locations of the reinforcing bar with magnified voids (light grey: concrete extruded after bar placement; dark grey: concrete extruded before bar placement): (a) reinforcing bar precisely at half the layer height; (b) reinforcing bar pushed into the lower layer; (c) reinforcing bar on top of the lower layer.

UniNa. The mortars used at the two institutions differed in the (i) initial yield strength, (ii) maximum aggregate size, and (iii) compressive strength. Due to the low initial yield strength and small aggregate size used at ETHZ, the mortar is expected to surround the reinforcing bar well, leading to a more homogeneous reinforcing bar covering. Furthermore, the higher compressive strength is known to result in increased bond strength. However, more detailed investigations are necessary to determine the exact influence of each of these parameters.

Considering the results from the material tests of the cut specimens (see Section 3.2.3), further observations can be made. During the cutting of specimen Z-R-3D⊥, the interface at the height of the reinforcement placement cracked, showing a weaker bond between the layers. However, this did not significantly influence the pull-out strength (Table 4 and Fig. 10). Hence, the tensile strength between the layers might have little influence on the overall bond between the reinforcing bar and the printed concrete. The neglectable reduction of the bending tensile strength between tested and untested specimens further shows that the produced stresses during pull-out of the reinforcing bar did not damage the interface.

As discussed in Section 3.4, the relative position between the bar and the filament could have slightly varied depending on the amount of material inside the formwork when printing the first 100 mm. The bar could end up either being placed halfway inserted as intended (Fig. 14a), all the way inserted due to material accumulation (Fig. 14b) or placed just on top of the layer due to a lack of material (Fig. 14c). These configurations could lead to a different void distribution and bar covering. The material capacity to fill these voids during printing depends on its viscosity. Indeed, a mortar with a low initial yield strength and small aggregate size can fill possible voids better than a high yield strength mortar, explaining the reduced scatter for the printing system of ETHZ compared to UniNa. This material property seems to have more influence in the parallel configuration than in the perpendicular one, for which the UniNa outcomes revealed higher scatter. The inspection of the concrete-steel interface did not show apparent voids around the reinforcing bar. However, it might be that these artefacts are not directly visible on this macroscopic scale.

The local pull-out bond failure at the interface with no cracking of the surrounding concrete can be explained by the printable mortar properties (strength and aggregate size) and the large confinement (small reinforcing bar diameter with respect to the specimens' size) that prevents splitting failures. In 3D concrete printing, the maximum aggregate size is typically smaller or equal to 2 mm (see Section 3.2), and the used reinforcing bars during the printing process have a small diameter. Therefore, the small aggregates in combination with small rib heights might facilitate the observed shearing behaviour. Hence, the bond behaviour and failure mode of reinforcing bars for 3D concrete printed elements might be determined by the mechanical behaviour and maximum aggregate size of the concrete together with the reinforcing bar diameter, with little influence of the production method. Further testing would be necessary to verify this observation, particularly for the case of robotically placed reinforcement.

4.5. Comparison to conventional concrete and previous 3DCP experiments

The comparison with respect to existing provisions and results for conventional concrete intends to explore if the anchorage and lap splice length of 3D concrete printed structures could be designed using existing code provisions [40,41]. For conventionally cast structures, many experimental data and bond models are available in the existing literature [40–42]. Codes, such as the *fib* Model Code 2010 [14] and the EN 1992-1-1 [43], typically provide the bond strength design value τ_{bd} for design purposes. Additionally, analytical bond shear stress-slip relationships are also provided in some cases for advanced modelling [14]. Fig. 15 compares the bond stress-slip relationships obtained in this study for the two investigated materials with the analytical laws provided in the *fib* Model Code 2010 [14], assuming good bond conditions and a pull-out failure. In detail, such an analytical law depends on the concrete mean compressive strength f_{cm} and the bar geometry (i.e. the clear distance between ribs). The main factor determining the maximum bond strength $\tau_{b,max}$ in the *fib* Model Code 2010, is the compressive strength. The bond strength in good bond conditions is $\tau_{max,good} = 2.5\sqrt{f_{cm}}$. For this comparison, an average bond stress-slip response of all tested configurations was calculated. The black curve in Fig. 15 shows the average relationship, while the grey area comprises all results.

The *fib* Model Code 2010 provides a slight underestimation of ca. 4 % of the bond strength for UniNa. Additionally, the analytical law is contained within the experimental scatter (see the grey area in Fig. 15a). On the contrary, the analytical model underestimates by 38 % the bond strength for ETHZ significantly. In both cases, the *fib* Model Code 2010 estimation for a 15 mm slip yielded a higher value of the residual bond stress than the experimental observations (+101 % and +70 %, for UniNa and ETHZ, respectively). Even though the compressive strength is considered in the prediction for Fig. 15, the *fib* Model Code 2010 highly underestimates the maximum bond strength for the printing system and material of ETHZ. Therefore, the low initial yield stress paired with the small maximum aggregate size seems to increase the bond strength significantly more than predicted in the model derived for concrete with larger aggregates.

The correlation between the bond and compressive strength is further analysed in Fig. 16 by comparing the results from this study to existing pull-out results in literature for 3D concrete printing, which used a similar testing set-up and reinforcement [24] and conventional concrete [44,45]. In Diab et al. [44] and Arel and Yazıcı [45], the maximum aggregate size was 19 and 22 mm, and the reinforcing bar diameters ranged from Ø16-18 mm and Ø10-14 mm, respectively. In addition to the experimental result, the relation proposed by the *fib* Model Code 2010 between compressive strength and maximum bond strength is plotted for good bond conditions and all other bond conditions ($\tau_{max,good}/2$) (red dashed lines in Fig. 16). It can be seen that the bond strength of conventionally cast concrete is enclosed within the boundaries proposed by *fib* Model Code 2010 for different bonding conditions. For the studies on 3D concrete printing, it is possible to observe that the analytical relation proposed in the *fib* Model Code 2010 tends to underestimate the bond strength for both cast and printed specimens (see the square and cross markers in Fig. 16, respectively). Such underestimation and the better performance resulting from 3DCP pull-out testing results is probably linked to (i) the difference in the cementitious formulation of printable materials with respect to the conventional concrete (e.g. aggregate size, cement content) and (ii) the small bar diameter used in 3DCP tests, rather than the fabrication method itself (note that cast and 3D printed yields similar results). It is worth noting that the inverse correlation between the bond strength and the bar diameter (point (ii) above) complies with the ACI CODE 318–08 [46] and the experimental data of Arel et al. [45].

Comparing the bond strength between 3D printing applications and conventional concrete demonstrates that the bond developed by manually placing reinforcement bars between the layers of printed concrete results in a better bond than conventional reinforced concrete. The best fit for 3D printable mortar is represented with the grey dashed line, i.e. $\tau_{b,max} = 4\cdot\sqrt{f_{cm}}$. However, the available experimental data is still limited, and further research is required to propose a reliable analytical law for 3DCP applications.

5. Pull-out behaviour of wire-reinforced samples

Table 5 and Fig. 17 show the average value of the maximum pull-out force for the specimens with wire reinforcement. The maximum pull-out force per unit length (F_{max}/l_b) ranges on average from 1.8 to 6.4 N/mm and from 5.3 to 11.8 N/mm for the printing system and material at UniNa and ETHZ, respectively. Assuming the equivalent diameter of 0.87 mm defined in Section 3.3, these results lead to a bond strength of 0.6–2.3 MPa at UniNa and 1.9–4.3 MPa at ETHZ. The bond strength of printed specimens compared to cast specimens was considerably lower at ETHZ and UniNa (i.e. 49% and 67%, respectively). Furthermore, in both institutes, the scatter in the results was much higher than in the tests with reinforcing bars. These results might be due to the difficulties of keeping the reinforcement straight during the specimen preparation (see Section 3.4).

The load-slip behaviour of each sample is depicted in Fig. 18 (no average was done in this case due to the wide scatter). It can be seen that in some cases, multiple local maxima were reached. Therefore, a point in the curves indicates the used maxima for the summary of results. The largest scatter could be observed for the cast specimens (W–C). While some cast specimens had a clear peak after the activation phase, other samples kept increasing the load after completing this phase. This wide variation might be attributed to a lack of straightness arising from the production process in the cast samples, which could lead to abnormally high friction forces.

At UniNa and ETHZ, the 3D printed samples showed significantly lower strength than the cast counterparts, independently of the printing orientation. However, the overall behaviour was similar regardless of the fabrication method. Since the wires were placed on top of the concrete during printing, straightness could be ensured. Hence, no deviation forces needed to be overcome in this case, which resulted in the wire being pulled out with less resistance than in the cast samples. At ETHZ, almost all 3D printed specimens had an initial stiff slope up to the peak, after which the wire started being pulled out. Only a little softening

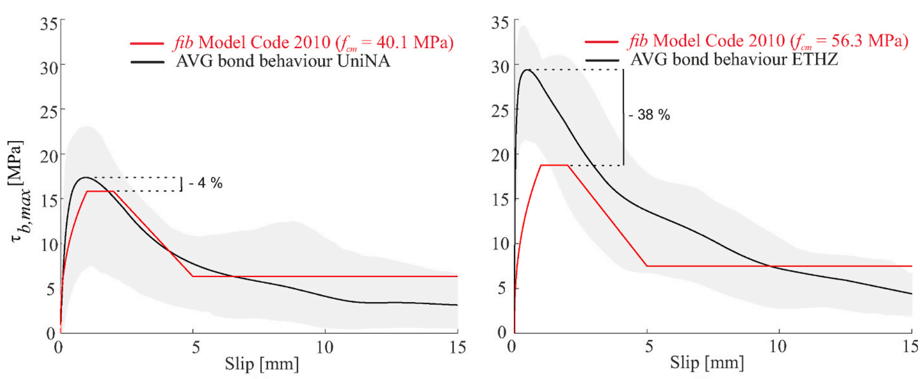

Fig. 15. Analytical [14] vs experimental bond stress-slip relationship: (a) UniNa and (b) ETHZ.

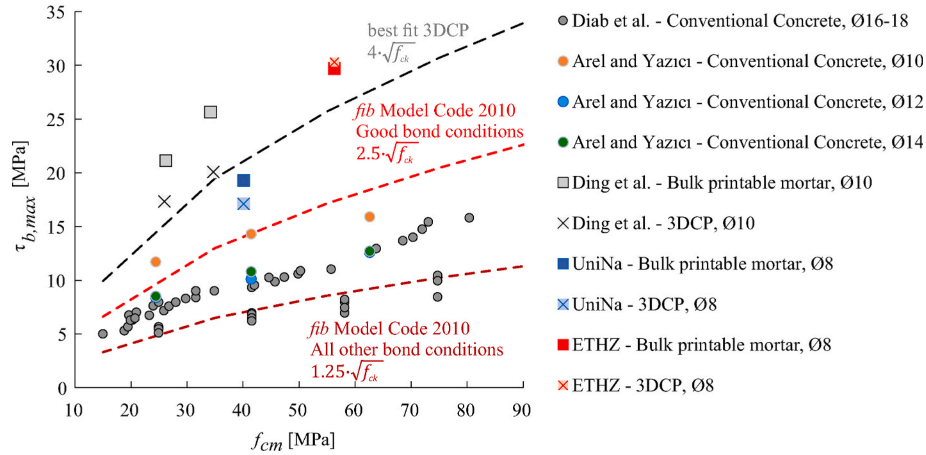

Fig. 16. Experimental correlations between compressive and bond strength [24,44,45] and analytical estimations of fib Model Code 2010 [40].

Table 5
Overview of pull-out test results for specimens with wire reinforcement (bond strength of wires calculated by assuming the equivalent diameter of 0.87 mm according to Section 3.3).

Codification	N–W–C	N–W-3D||	N–W-3D⊥	Z-W-C	Z-W-3D||	Z-W-3D⊥
F_{max}/l_b [N/mm]	6.4	1.8	2.5	11.8	5.3	6.8
(CoV)	(52%)	(42%)	(27%)	(32%)	(16%)	(21%)
F_{max} [N]	320	88	124	590	266	339
$\tau_{b,max}$ [MPa]	2.3	0.6	0.9	4.3	1.9	2.5

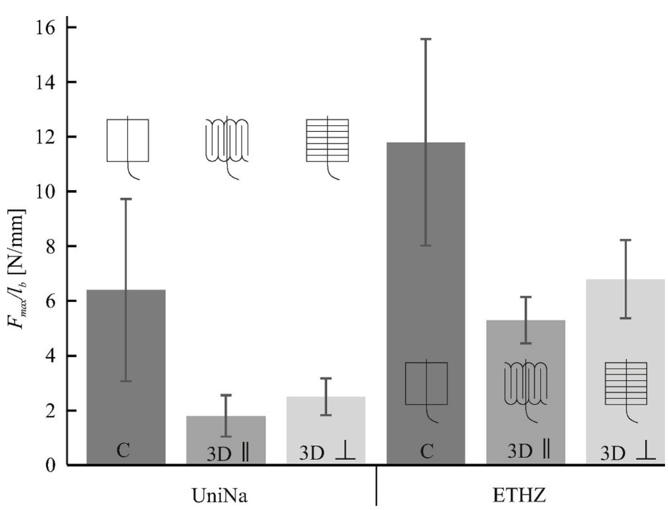

Fig. 17. Graphical representation of the pull-out tests' mean strength and coefficient of variation for specimens with wire reinforcement.

occurred after the activation for the slip range displayed in Fig. 18 (ca. twice the wire diameter). At UniNa, the initial hardening during the activation phase could also be observed, but the typical softening response during the wire pull-out could only be observed for slip values above twice the wire diameter. The behaviour of the 3D printed samples is related to the smoothness of the wire. This smoothness leads to the pull-out being dominated by the friction between steel and concrete, without any interlocking provided by the ribs on the reinforcing bars. This behaviour resembles the response of plain bars, in which a chemical bond dominates the initial stiff response. Once this bond fails, pull-out dominated by friction occurs [40].

During cutting for the material tests (see Section 3.2.3), the inspected specimen from configuration Z-W-3D|| cracked along the interface in which the reinforcement was placed. It should be noted that the time interval for reinforcement placing in this configuration (9 min) was almost double that in the other cases (5.5 min), which seems to be too high to ensure a good interlayer bond for the accelerated mix. However, this did not significantly influence the pull-out force (see configuration Z-W-3D|| in Table 5 and Fig. 17). This result suggests that the pull-out behaviour of the wires is independent of the bonding between the printed layers.

Compared to the study by Bos et al. [27], the behaviour and peak load for pull-out tests were similar. Their study used two types of high-strength steel wires with multiple strands with a nominal diameter of 1.0 and 1.2 mm (i.e. similar to the wire used in this study). For the parallel configuration, an average peak value of 1.8 N/mm and 5.3 N/mm was reached at UniNa and ETHZ, respectively. In the work of Bos et al. [27], values in the range of 2.2 to 8.1 N/mm were reached for an embedment length ranging from 35 to 200 mm. The largest bond strength observed by Bos et al. [27] was for a short embedment length (35 mm) with the smaller wire (i.e. 1.0 mm in diameter). The wire was pulled out in both studies, reaching tensile stresses much lower than its ultimate strength. The wire used in this study would require activating a bond of ca. 26 N/mm over a 50 mm embedment length to break the wire (i.e. the wire stress was always below 25% of its strength). The difficulties in anchoring the wires properly and reaching a reasonable utilisation level pose questions about the applicability of wires for reinforcing 3D concrete printing. Using this reinforcement approach would require exploring alternative measures to solve the anchorage geometrically (i.e. anchorage due to change in direction). This alternative approach was already explored by Gebhard et al. [9]. In this study, the wires were used as shear reinforcement and bent similarly to stirrups. During experimental testing, the breakage of the wires was reached thanks to the proper anchorage by means of the change in wire direction. For large scale structures, such or a similar anchorage would need to be provided to make the wires a feasible reinforcement solution.

6. Insights towards standardisation

This study has shown an attempt to determine the bond strength between 3D concrete printing and reinforcement manually placed between the printed layers in two institutes using homogeneous testing conditions. This section summarises the main findings of this comparative study in the context of the ongoing research effort to standardise the bond properties of the reinforcement in 3D concrete printing structural applications. For the specimens reinforced with wires, the large scatter of the results suggests that the chosen production and test set-up were not ideal for obtaining repeatable results. Therefore, this section focuses on the test procedure for rigid and straight reinforcement

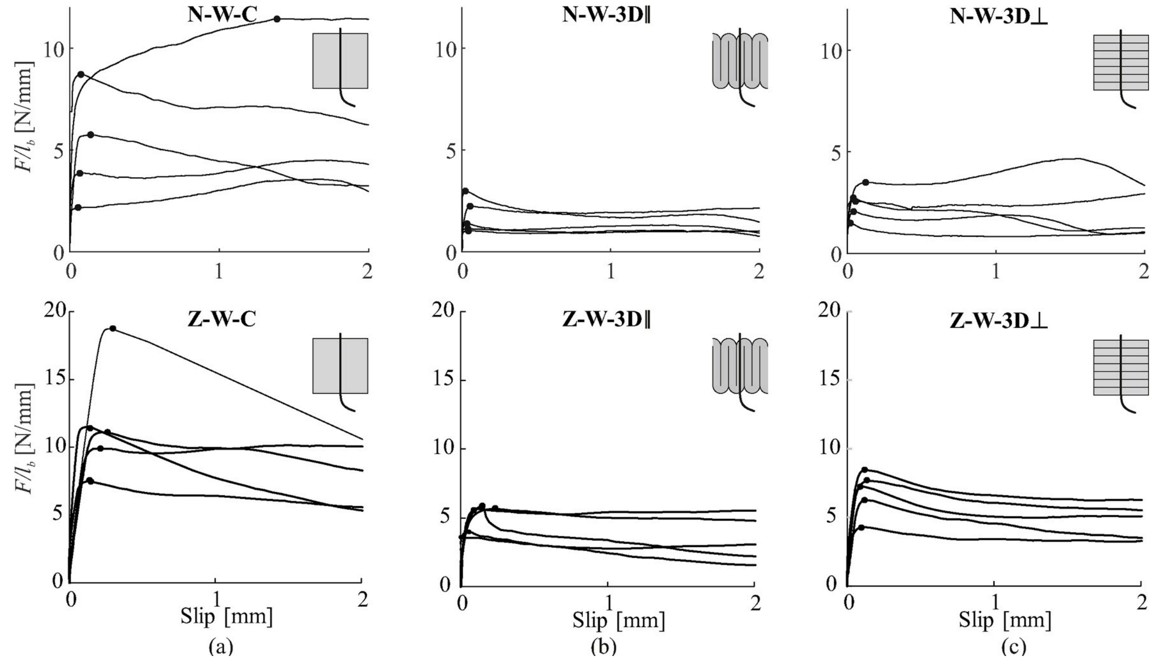

Fig. 18. Bond slip behaviour of the pull-out tests with wire reinforcement (top: ETHZ printing set-up; bottom: Napoli printing set-up): (a) cast specimens; (b) 3D printed specimens with the parallel configuration; (c) 3D printed specimens with the perpendicular configuration.

bars.

As mentioned in the introduction, various studies used different approaches to produce pull-out specimens from 3D printed elements. Compared to the other approaches, the samples were entirely printed inside a formwork in this study without additional casting or cutting steps. While the formwork could slightly affect the concrete properties close to the specimen's edge, the bond behaviour is not expected to be affected, provided the embedment length is located with a sufficient cover. The printing inside a formwork approach had the advantages to (i) control the geometry of the specimens and ensure straight surfaces for the load introduction, (ii) control precisely the location of the reinforcement by placing it in a hole in the formwork, and (iii) cut the specimen in a fresh state if a small spacing between consecutive formworks is provided. The main limitation of this production was that the final position of the reinforcement relative to the concrete could not be precisely controlled as it depended on small materials accumulation during printing (see Section 4.2). Furthermore, this approach is limited to non-rotation nozzles with a symmetric opening. For rotating nozzles, the space between the formwork walls might not be sufficient to fill the formwork properly. Therefore, another approach might be needed for rotating nozzles, especially for the reinforcement placed in the same direction as the printing path. However, the authors still consider this formwork approach valuable whenever applicable since it offers a straightforward and well-controlled production process.

Another relevant aspect for the standardisation of bond tests relates to the used reinforcement diameter and isolation elements. The RILEM recommendation for pull-out tests [13] prescribes an isolation element with 1 mm tolerance around the bar and a thickness of less than 2 mm on the side where the bar is pulled. However, for 3D concrete printing, the height of the reinforcing bar and the isolation element that can stand out of the lower printed layer is limited by the chosen layer height and material consistency to avoid a collision with the nozzle when printing the following layer. Assuming that half of the reinforcement is embedded in the bottom layer, the total diameter of the reinforcing bar and isolation is limited by double the layer height. For printable materials with high initial yield strength, it is difficult to achieve high printing qualities for low layer heights (i.e. below 5 mm), while a larger layer height (i.e. 10 mm and more) is challenging with fluid set-on demand materials. In this study, the layer height was chosen at 7 mm to allow a high printing quality at both institutes. This layer height limits the reinforcing bar diameter to 8 mm when using an isolation pipe of 2 mm thickness with 1 mm tolerance. The study of the bond behaviour of reinforcing bars of larger diameters would require adjusting the printing parameters. This adjustment might, in turn, affect the bond behaviour, hindering the characterisation of the bond properties with a limited number of tests.

A final remark should be made about the representability of the conducted studies with manually placed reinforcement for future applications with robotic reinforcement placement (required for large scale applications). It would need to be ensured that the quality of the automated placement is high enough to ensure the same mechanical response as the standardised tests on manually placed reinforcement. For this matter, additional tests should be performed to ensure that the standardised specimens correlate with the automatically placed ones.

7. Conclusion

The authors of this paper planned and performed an identical experimental campaign in two different laboratories (UniNa and ETHZ) to investigate the bond behaviour of steel reinforcement manually inserted in 3D printed concrete elements. In the innovative field of digital fabrication with concrete, interlaboratory studies can be useful towards the standardisation of testing procedures, highlighting difficulties, challenges and possible solutions to define a simple and reliable experimental method.

The results showed that the reinforcement failed due to pull-out without generating splitting cracks in the surrounding matrix. The straight wires exhibited poor bond and a large scatter in the results. The experimental results of reinforcing steel bars showed that:

- The reinforcing bars are well covered by the printed mortars, and no oblivious defects are introduced by the printing process.
- There is no difference in the bond behaviour between printed and cast specimens for the printing system and material at ETHZ.
- The printed specimens with the reinforcement parallel to the printing direction showed the largest scatter.

- The printing strategy of UniNa achieved a lower bond strength than the one of ETHZ. The main differences of the set-on demand printing approach used at ETHZ compared to the high yield strength printing approach used at UniNa (i.e. reduced initial yield strength, smaller aggregate size and higher compressive strength) all seem to have a positive effect on the bond strength.

Comparison to conventional concrete and existing models showed that:

- The bond between reinforcing bars and 3D printable mortars is generally higher than for conventional concrete of the same compressive strength. Therefore, traditional models underestimate the bond strength of 3D concrete printed mortars.
- This observation is probably due to the composition of the printable mortars (e.g. small aggregate size and large cement content) and the small reinforcing bar diameters used in 3D concrete printing.

This interlaboratory study showed the importance of collaborative research for 3D concrete printing. The structural behaviour of the produced elements depends not only on the chosen concrete quality but also on the applied production and testing strategy. This dependence requires further attention since it is essential to understand these influences to develop standards and design codes accounting for the particularities of 3D concrete printed structures. The study offered meaningful insights into the influence of bond behaviour due to the fabrication method and material used. However, to apply these reinforcement strategies for load-bearing structures, further considerations such as automation of the reinforcement placement and durability need to be considered.

Author statement

The first two authors of this article contributed equally.

Lukas Gebhard: Conceptualisation, Methodology, Formal analysis, Investigation, Data Curation, Writing - Original Draft, Writing - Review & Editing; **Laura Esposito**: Conceptualisation, Methodology, Formal analysis, Investigation, Data Curation, Writing – Original Draft, Writing - Review & Editing; **Costantino Menna**: Conceptualisation, Methodology, Writing - Review & Editing, Supervision; **Jaime Mata-Falcón**: Conceptualisation, Methodology, Writing - Review & Editing, Supervision.

Open-access data repository

The data for the present publication can be found under the following DOI: https://doi.org/10.3929/ethz-b-000556740.

Declaration of competing interest

The authors declare that they have no known competing financial interests or personal relationships that could have appeared to influence the work reported in this paper.

Acknowledgements

The authors would like to thank the team of Etesias (Napoli, Italy) and Ana Anton (Digital Building Technologies, ETH Zurich) and Lex Reiter (Chair of Physical Chemistry of Building Materials, ETH Zurich) for their support in the printing laboratory. Furthermore, the authors are grateful for the support of the two teams of the structural labs at both institutes. At ETH Zurich, the experimental campaign was funded, and the exchange was supported by the Swiss National Science Foundation, within the National Centre for Competence in Research in Digital Fabrication (project number 51NF40-141853). At UniNa, the experimental activities were supported by Italcementi Heidelberg Cement Group (industrial partner of the PhD program) and by the Italian Ministry of University and Research (MIUR) under program PON 2014–2020 (CCI 2014IT16M2OP005). A special thanks for enabling the exchange and supporting the research goes to Prof. Dr. Walter Kaufmann (ETH Zurich).

References

[1] O. Ortiz, F. Castells, G. Sonnemann, Sustainability in the construction industry: a review of recent developments based on LCA, Construct. Build. Mater. 23 (2009) 28–39, https://doi.org/10.1016/j.conbuildmat.2007.11.012.
[2] B. Khoshnevis, Automated construction by contour crafting—related robotics and information technologies, Autom. ConStruct. 13 (2004) 5–19, https://doi.org/10.1016/j.autcon.2003.08.012.
[3] S.C. Paul, G.P.A.G. van Zijl, M.J. Tan, I. Gibson, A review of 3D concrete printing systems and materials properties: current status and future research prospects, Rapid Prototyp. J. 24 (2018) 784–798, https://doi.org/10.1108/RPJ-09-2016-0154.
[4] T. Wangler, N. Roussel, F.P. Bos, T.A.M. Salet, R.J. Flatt, Digital concrete: a review, Cement Concr. Res. 123 (2019), 105780, https://doi.org/10.1016/j.cemconres.2019.105780.
[5] D. Asprone, C. Menna, F.P. Bos, T.A.M. Salet, J. Mata-Falcón, W. Kaufmann, Rethinking reinforcement for digital fabrication with concrete, Cement Concr. Res. 112 (2018) 111–121, https://doi.org/10.1016/j.cemconres.2018.05.020.
[6] H. Kloft, M. Empelmann, N. Hack, E. Herrmann, D. Lowke, Reinforcement strategies for 3D-concrete-printing, Civil Engineering Design 2 (2020) 131–139, https://doi.org/10.1002/cend.202000022.
[7] V. Mechtcherine, R. Buswell, H. Kloft, F.P. Bos, N. Hack, R. Wolfs, et al., Integrating reinforcement in digital fabrication with concrete: a review and classification framework, Cement Concr. Compos. (2021), 103964, https://doi.org/10.1016/j.cemconcomp.2021.103964.
[8] C. Menna, J. Mata-Falcón, F.P. Bos, G. Vantyghem, L. Ferrara, D. Asprone, et al., Opportunities and challenges for structural engineering of digitally fabricated concrete, Cement Concr. Res. 133 (2020), 106079, https://doi.org/10.1016/j.cemconres.2020.106079.
[9] L. Gebhard, J. Mata-Falcón, A. Anton, B. Dillenburger, W. Kaufmann, Structural behaviour of 3D printed concrete beams with various reinforcement strategies, Eng. Struct. 240 (2021), 112380, https://doi.org/10.1016/j.engstruct.2021.112380.
[10] M. Alawneh, M. Matarneh, S. El-Ashri, THE WORLD'S FIRST 3D–PRINTED OFFICE BUILDING IN DUBAI, 19, 2018.
[11] V. Mechtcherine, A. Michel, M. Liebscher, T. Schmeier, Extrusion-based additive manufacturing with carbon reinforced concrete: concept and feasibility study, Materials 13 (2020) 2568, https://doi.org/10.3390/ma13112568.
[12] F.P. Bos, Z.Y. Ahmed, E.R. Jutinov, T.A. Salet, Experimental exploration of metal cable as reinforcement in 3D printed concrete, Materials 10 (2017) 1314.
[13] RILEM TC. RC 6 Bond test for reinforcement steel. 2. Pull-out test, 1983, RILEM Recommendations for the Testing and Use of Constructions Materials, E & FN Spon, London, 1994, pp. 218–220.
[14] fib Model Code 2010. Fib Model Code for Concrete Structures 2010 2013.
[15] B.S. Hamad, Comparative bond strength of coated and uncoated bars with different rib geometries, MJ 92 (1995) 579–590, https://doi.org/10.14359/9776.
[16] G. Metelli, G.A. Plizzari, Influence of the relative rib area on bond behaviour, Mag. Concr. Res. 66 (2014) 277–294, https://doi.org/10.1680/macr.13.00198.
[17] F. Moccia, M. Fernández Ruiz, G. Metelli, A. Muttoni, G. Plizzari, Casting position effects on bond performance of reinforcement bars, Struct. Concr. 22 (2021) 1612–1632, https://doi.org/10.1002/suco.202000572.
[18] Z.P. Bazant, Siddik Sener, Size effect in pullout tests, ACI Mater. J. (1987) 85. M38.
[19] Y. Lemcherreq, T. Galkovski, J. Mata-Falcón, W. Kaufmann, Application of distributed fibre optical sensing in reinforced concrete elements subjected to monotonic and cyclic loading, Sensors 22 (2022) 2023, https://doi.org/10.3390/s22052023.
[20] F. Brantschen, D.m. v. Faria, M. Fernández Ruiz, A. Muttoni, Bond behaviour of straight, hooked, U-shaped and headed bars in cracked concrete, Struct. Concr. 17 (2016) 799–810, https://doi.org/10.1002/suco.201500199.
[21] T. Galkovski, Y. Lemcherreq, J. Mata-Falcón, W. Kaufmann, Fundamental studies on the use of distributed fibre optical sensing on concrete and reinforcing bars, Sensors 21 (2021) 7643, https://doi.org/10.3390/s21227643.
[22] B. Baz, G. Aouad, S. Remond, Effect of the printing method and mortar's workability on pull-out strength of 3D printed elements, Construct. Build. Mater. 230 (2020), 117002, https://doi.org/10.1016/j.conbuildmat.2019.117002.
[23] B. Baz, G. Aouad, P. Leblond, O. Al-Mansouri, M. D'hondt, S. Remond, Mechanical assessment of concrete – steel bonding in 3D printed elements, Construct. Build. Mater. 256 (2020), 119457, https://doi.org/10.1016/j.conbuildmat.2020.119457.
[24] T. Ding, F. Qin, J. Xiao, X. Chen, Z. Zuo, Experimental study on the bond behaviour between steel bars and 3D printed concrete, J. Build. Eng. 49 (2022), 104105, https://doi.org/10.1016/j.jobe.2022.104105.
[25] X. Sun, C. Gao, H. Wang, Bond performance between BFRP bars and 3D printed concrete, Construct. Build. Mater. 269 (2021), 121325, https://doi.org/10.1016/j.conbuildmat.2020.121325.
[26] N. Freund, D. Lowke, Interlayer reinforcement in shotcrete-3D-printing : the effect of accelerator dosage on the resulting bond behavior of integrated reinforcement bars, Open Conf. Proceed. 1 (2022) 83–95, https://doi.org/10.52825/ocp.v1i.72.

[27] F. Bos, S. Dezaire, Z. Ahmed, A. Hoekstra, T. Salet, Bond of reinforcement cable in 3D printed concrete, in: F.P. Bos, S.S. Lucas, R.J.M. Wolfs, T.A.M. Salet (Eds.), Second RILEM International Conference on Concrete and Digital Fabrication, Springer International Publishing, Cham, 2020, pp. 584–600, https://doi.org/10.1007/978-3-030-49916-7_60.

[28] L. Reiter, T. Wangler, A. Anton, R.J. Flatt, Setting on demand for digital concrete – principles, measurements, chemistry, validation, Cement Concr. Res. 132 (2020), 106047, https://doi.org/10.1016/j.cemconres.2020.106047.

[29] T.T. Le, S.A. Austin, S. Lim, R.A. Buswell, A.G.F. Gibb, T. Thorpe, Mix design and fresh properties for high-performance printing concrete, Mater. Struct. 45 (2012) 1221–1232, https://doi.org/10.1617/s11527-012-9828-z.

[30] S. Paul, Y. Wei, Y.W.D. Tay, B. Panda, M.J. Tan, Fresh and hardened properties of 3D printable cementitious materials for building and construction, Arch. Civ. Mech. Eng. 18 (2017), https://doi.org/10.1016/j.acme.2017.02.008.

[31] N. Roussel, Rheological requirements for printable concretes, Cement Concr. Res. 112 (2018), https://doi.org/10.1016/j.cemconres.2018.04.005.

[32] Standards E, UNE EN 196-3:2017 Methods of testing cement - Part 3: determination of setting times and soundness, Https://WwwEn-StandardEu n.d, https://www.en-standard.eu/une-en-196-3-2017-methods-of-testing-cement-part-3-determination-of-setting-times-and-soundness/. (Accessed 17 March 2022).

[33] Standard test method for flow of hydraulic cement mortar n.d. https://www.astm.org/c1437-20.html. (Accessed 17 March 2022).

[34] Pierre A, Lanos C, Estellé P. Extension of Spread-Slump Formulae for Yield Stress Evaluation n.D.:23.

[35] EN 12390-3:2019, Testing hardened concrete - Part 3: compressive strength of test specimens. ITeh Standards Store n.d. https://standards.iteh.ai/catalog/standards/cen/7eb738ef-44af-436c-ab8e-e6561571302c/en-12390-3-2019. (Accessed 21 May 2021).

[36] Standard test method for splitting tensile strength of cylindrical concrete specimens n.d. https://www.astm.org/c0496-96.html. (Accessed 17 March 2022).

[37] EN 196-1:2016 - Methods of Testing Cement - Part 1: Determination of Strength 2016.

[38] R.J.M. Wolfs, F.P. Bos, T.A.M. Salet, Hardened properties of 3D printed concrete: the influence of process parameters on interlayer adhesion, Cement Concr. Res. 119 (2019) 132–140, https://doi.org/10.1016/j.cemconres.2019.02.017.

[39] A. Anton, L. Reiter, T. Wangler, V. Frangez, R.J. Flatt, B. Dillenburger, A 3D concrete printing prefabrication platform for bespoke columns, Autom. ConStruct. 122 (2021), 103467, https://doi.org/10.1016/j.autcon.2020.103467.

[40] R. Tepfers, Z. Achillides, A. Azizinamini, G. Balázs, A. Bigaj-van-Vliet, J. Cabrera, et al., Fib Bulletin 10. Bond of Reinforcement in Concrete. Fib, The International Federation for Structural Concrete, 2000, https://doi.org/10.35789/fib.BULL.0010.

[41] Eurocode 2: design of concrete structures (EN 1992). https://www.ds.dk/en/our-services/eurocodes/technical-standards/eurocode-2, 2004. (Accessed 30 September 2021).

[42] Ferguson (chairman) AC 408 PM, Bond stress-the state of the art, JP 63 (1966) 1161–1190, https://doi.org/10.14359/7665.

[43] EN 1992-1-1 2004 Eurocode 2: Design of Concrete Structures - Part 1-1: General Rules and Rules for Buildings n.D.

[44] A.M. Diab, H.E. Elyamany, M.A. Hussein, H.M. Al Ashy, Bond behavior and assessment of design ultimate bond stress of normal and high strength concrete, Alex. Eng. J. 53 (2014) 355–371, https://doi.org/10.1016/j.aej.2014.03.012.

[45] H. Arel, Ş. Yazıcı, The Effect of Different Parameters on the Concrete -bar Bond, 22, 2015.

[46] ACI CODE 318-08: building code requirements for structural concrete and commentary n.d. https://www.concrete.org/store/productdetail.aspx?ItemID=31808&Language=English&Units=US_Units. (Accessed 3 March 2022).